



**HAL**  
open science

## Damage detection of glass fiber reinforced composites using embedded PVA-carbon nanotube (CNT) fibers

N.D. Alexopoulos, C. Bartholome, P. Poulin, Z. Marioli-Riga

► **To cite this version:**

N.D. Alexopoulos, C. Bartholome, P. Poulin, Z. Marioli-Riga. Damage detection of glass fiber reinforced composites using embedded PVA-carbon nanotube (CNT) fibers. *Composites Science and Technology*, 2010, 70 (12), pp.1733-1741. 10.1016/j.compscitech.2010.07.004 . hal-00671655

**HAL Id: hal-00671655**

**<https://hal.science/hal-00671655>**

Submitted on 18 Feb 2012

**HAL** is a multi-disciplinary open access archive for the deposit and dissemination of scientific research documents, whether they are published or not. The documents may come from teaching and research institutions in France or abroad, or from public or private research centers.

L'archive ouverte pluridisciplinaire **HAL**, est destinée au dépôt et à la diffusion de documents scientifiques de niveau recherche, publiés ou non, émanant des établissements d'enseignement et de recherche français ou étrangers, des laboratoires publics ou privés.

## Accepted Manuscript

Damage detection of glass fiber reinforced composites using embedded PVA-carbon nanotube (CNT) fibers

N.D. Alexopoulos, C. Bartholome, P. Poulin, Z. Marioli-Riga

PII: S0266-3538(10)00261-7  
DOI: [10.1016/j.compscitech.2010.07.004](https://doi.org/10.1016/j.compscitech.2010.07.004)  
Reference: CSTE 4758

To appear in: *Composites Science and Technology*

Received Date: 17 February 2010  
Revised Date: 1 July 2010  
Accepted Date: 4 July 2010

Please cite this article as: Alexopoulos, N.D., Bartholome, C., Poulin, P., Marioli-Riga, Z., Damage detection of glass fiber reinforced composites using embedded PVA-carbon nanotube (CNT) fibers, *Composites Science and Technology* (2010), doi: [10.1016/j.compscitech.2010.07.004](https://doi.org/10.1016/j.compscitech.2010.07.004)

This is a PDF file of an unedited manuscript that has been accepted for publication. As a service to our customers we are providing this early version of the manuscript. The manuscript will undergo copyediting, typesetting, and review of the resulting proof before it is published in its final form. Please note that during the production process errors may be discovered which could affect the content, and all legal disclaimers that apply to the journal pertain.



# Damage detection of glass fiber reinforced composites using embedded PVA-carbon nanotube (CNT) fibers

N.D. Alexopoulos<sup>1,2,\*</sup>, C. Bartholome<sup>3</sup>, P. Poulin<sup>3</sup> and Z. Marioli-Riga<sup>1</sup>

<sup>1</sup>*Hellenic Aerospace Industry, Research and Development Department, 320 09 Schimatari, Greece*

<sup>2</sup>*University of the Aegean, Department of Financial and Management Engineering, 821 00 Chios, Greece*

<sup>3</sup>*Université de Bordeaux, Centre de Recherche Paul Pascal – CNRS, Avenue Schweitzer, 33600 Pessac, France*

## Abstract

In the present work, polyvinyl alcohol carbon nanotube (PVA-CNT) fibers were embedded in glass fiber reinforced plastic composites and used as strain sensors for damage monitoring of the composite. Sensing of the structural integrity of the composite was made by the in-situ measurement of the electrical resistance of the embedded PVA-CNT fiber during the mechanical tests. The multi-functionable materials were tested in tensile progressive damage accumulation (PDA) tests. These tests aimed to seek the electrical response of untreated and pre-stretched PVA-CNT fibers with known level of progressively introduced damage to the composite. The advantages and disadvantages of each PVA-CNT fiber used as a sensor are analyzed; the electrical resistance readings of the PVA-CNT fibers were correlated with known parameters that express the induced damage of the composite.

*Keywords:* A. Carbon nanotubes, A. Glass fibres, A. Smart materials, B. Electrical properties, B. Mechanical properties

## 1. Introduction

Composite materials and structures offer great advantages, e.g. specific mechanical properties, when compared to their competitive materials. Their main disadvantage to be used in civil aircraft structures is their non-destructive testing (NDT) or their in-situ identification of developed non-visible damage under real loading conditions. Research in such direction is of imperative importance for their wide use in a/c structures. In such conditions, inspection and maintenance periods are often very critical and a methodology is needed to minimize the time intervals that the

---

\* Corresponding author : [nalexop@tee.gr](mailto:nalexop@tee.gr)

components are out-of service. An in-situ structural health monitoring system would primarily give on-line information regarding the structural safety of the structure and secondarily would significantly lower the inspection / maintenance costs.

An intelligent structural health monitoring system could provide firstly on-line information on the developed damage to a specific location of the composite structure and secondarily its extend. Typical state-of-the-art damage and sensing techniques are the active piezoelectric sensors, fibre optical sensors and acoustic emission sensors, e.g. [1] to [3]. These techniques have been applied to composite materials and structures by using embedded sensors. Nevertheless, each technique presents specific advantages and disadvantages that will be shortly discussed.

Embedded piezoelectric sensors have been used in the literature to detect damage in composite materials and structures. This technique uses a wave field generated by an actuator and propagates into the composite. The mechanical waves are detected by other integrated sensors, and thus allowing for a structural analysis and the detection of damage. Damage can also be detected by similar methods, e.g. ultrasonic lamb waves [1],[5], or impedance spectroscopy, e.g. [6],[7]. In [8] to [12] it was shown that different types of damage influence strongly the propagation of such mechanical waves. However, their drawbacks are essential; the embedded sensors downgrade the fatigue life of the composite [8], while the embedded sensors might be damaged by the applied pressure values during the manufacturing process cycle (e.g. autoclave process) of the composites.

Another technique for the damage monitoring of composite materials is the embedded glass fibre optical sensors. Damage detection can be realized by a breakage of the optical fibre, resulting in a loss of a transmitted light signal [13] or by mechanical coupling, where a change in local strain leads to a change in the coefficient of refraction [14]. The detection of these changes can be used for SHM in composites by an interferometric system or by small embedded Bragg grating sensors, e.g. [15] to [17]. The assessment of small defects, e.g. the transverse matrix cracks is a main drawback of this technique to be used in composites. In order to provide a reliable detection, a dense network of optical fibres would be needed, which might firstly complicate manufacturing, and secondarily increase the material's costs. In addition, the presence of optical fibres degrades the mechanical performance of the laminate, as typical optical fibres exhibit diameters 5-10 times higher than the reinforcing fibres. Therefore, they act as defects in the reinforcing structure [18] and may decrease the crack initiation threshold [19].

Another technique to monitor damage development in composite laminates is the acoustic emission (AE). The initiation of damage such as matrix cracking, delamination and fibre breakage are accompanied by a distinct acoustic effect, which can be recorded via transducer sensors. The acoustic events can therefore be directly linked to a specific type of failure or can be evaluated in a cumulative manner to characterize the state of damage of the composite, e.g. [20] to [24]. The AE

data are usually not sufficient to solely characterize the condition of the composite; this technique was proven to be quite powerful in experimental studies and a valuable addition to other health monitoring techniques [20].

All existing sensor technologies for composite health monitoring all appear to have their individual limitations concerning resolution or clearness of the measured data. Furthermore, cost intensive external hardware is needed and for fibre optical and piezoelectric sensors, the sensor hardware has to be embedded into the composite structure. This has been proven to be detrimental to the composite properties. Furthermore, the introduction of health monitoring systems should be compatible with existing composite manufacturing processes. This is especially difficult in the case of embedded piezoelectric sensors or MEMS, as these devices are sensitive to high temperatures and pressures.

In the present work, a new type of embedded sensor for damage monitoring of composites is assessed. Using the electrical conductivity of embedded nano-fibers into non-conductive composites, the structural health monitoring can be assessed by the in-situ measurements of the electrical resistance change of the nano-fiber. Notice that the monitoring of carbon fibre composites that have inherent conductivity has been performed the last two decades, e.g. [25] to [27]. The idea of monitoring a composite using a unique fiber has been made in [28], where a carbon fiber was embedded into GFRP. Mainly due to the difference in modulus of elasticity between the two medias, the sensor 'carbon fiber' didn't monitor the progressive damage of the composite but actually prognosed its final fracture. In a previous work [29], the authors showed that polyvinyl alcohol carbon nanotube (PVA-CNT) fibers produced residual resistance after every unloading step. In the present work, these fibers have been pre-stretched before being using as sensors. Damage of the composite was directly correlated to the PVA-CNT fiber readings for both, untreated and pre-stretched fibers. Advantages and disadvantages of each embedded fiber is analyzed and discussed.

## **2. Material manufacturing**

The materials used for the manufacture of the flat composite material plates with embedded PVA-carbon nanotube (CNT) fibers were (a) multi-wall carbon nanotubes that were used to prepare the PVA-CNT fibers with a coagulation process, (b) epoxy resin Araldite LY564 / hardener Aradur 2954 supplied by Huntsman Advanced Materials, Bergkamen, Germany (ratio 100:35 parts by weight) and (c) glass fiber fabric PW, Style 6781 (S2-glass) by Fiber Glast Developments Corporation.

## 2.1 Carbon nanotube fiber

The PVA-CNT fiber manufacturing process consisted in injecting an aqueous carbon nanotube dispersion into the co-flowing stream of a coagulating polyvinyl alcohol solution. The nanotube dispersion is stabilized by sodium dodecyl, an anionic surfactant. The PVA polymer was purchased from Seppic – France. It has a molecular weight of 195000 g/mol and a hydrolysis ratio of 99%. More details regarding the manufacturing process of the fiber can be seen in [30]-[32]. A scanning electron image of the produced carbon nanotube fiber can be seen in Figure 1. Such a fiber contains a weight fraction of nanotubes of about 15wt%. The first trial of the CNT fiber was used as an embedded strain sensor in GFRP composites [29]. Typical resistance – strain correlation of the CNT fiber (hereafter will be called untreated) can be seen in Figure 2. The experimental curve of the untreated fiber exhibits a non monotonic behaviour of decreasing and increasing resistance at low and high strains, respectively. For the values of strain higher than 20%, there exists a continuous increase in resistance with increasing strain of the PVA-CNT fiber.

More recently, investigations on the PVA-CNT fiber using Raman spectroscopy showed that the fiber exhibit an elastic behaviour under tensile loads and at the first stages of deformation [33]. The untreated fiber is working due to shifting of the carbon nanotubes when stretched up to its elastic regime. When exceeded this stretching value, irreversible plastic deformation is introduced to the PVA fiber, which was evident for the case of the hybrid composite material [29]. A typical loading – unloading case of this hybrid material for strain higher than the elastic regime of the fiber can graphically be seen in Figure 3. The formation of hysteresis loop as well as the observed residual resistance of the fiber after every unloading was increasing with increasing the incremental loading level. It was demonstrated that these values were mainly attributed to damage in the PVA-CNT fiber but it is mentioned that it could be calibrated to quantify the introduced damage of the composite due to mechanical loading.

In order to avoid this phenomenon, a pre-stretching of the fiber was decided to improve the mechanical properties of the fibers and thereby decreases its tendency to be damaged when it is used as sensor. Note that a typical elongation of a GFRP material is of the order of 5%, while the maximum elongation of the fiber exceeds 100%. Stretching of the fibers was performed at the approximate level of 20% and hereafter the new fibers will be called *pre-stretched* fibers.

## 2.2 Composite plates with embedded CNT fibers

The manufacturing of the hybrid composite material was made at Hellenic Aerospace Industry (HAI) and was extensively described elsewhere [29]. Briefly, 10 plies of fabric, oriented at 0/90°

had been cut at the required dimensions (300 x 300 mm). The first 9 plies were laid and the wrap faces were alternated upwards and downwards during the lay-up, resulting in a cross-ply balanced and symmetric laminate. The PVA-CNT fibers were placed between the 9<sup>th</sup> and last ply of the composite. In total six PVA-CNT fibers were used per manufactured composite plate; this permitted the manufacturing of six testing specimens with one embedded fiber per specimen.

The specimens with the PVA-CNT fiber had been cut from the material plates according to the ASTM D3039 specification and edge-polished. The dimensions of the testing specimens were width x length = 25 mm x 250 mm. At the two marks of each specimen covered with silver paste, two cable connectors had been added again with silver paste in order to attach the multimeter for the resistance measurements.

### 3. Experimental procedure

Monotonic tensile and incremental tensile loading – unloading steps had been performed to evaluate the hybrid materials. A servo-hydraulic Instron 100 kN testing machine had been used to record the force and displacement data, while a 50 mm extensometer was attached to record axial strain data of the coupons. Additionally an Agilent multimeter was used to record in situ the electrical resistance data at a rate of 1 Hz of the specimen's embedded PVA-CNT fiber during mechanical loading. More details about the experimental procedure can be seen in [29].

Different quasi-static incremental loading – unloading steps in different specimens had been made to seek the fiber's response. As the incremental loading steps had been made to specific levels of tensile fracture stress of the material, the testing machine was load-controlled. Unloading of the specimen had been made at the zero loading state of the machine.

## 4. Results and discussion

### *4.1 Effect of the CNT fiber on the structural integrity of the composite*

Embedding the PVA-CNT fiber into the composite is not a straight forward procedure; as the conductive fiber should somehow be recorded on the surface of the composite, there is a possibility to induce artificial defects on the material. Tensile as well as progressive damage accumulation (PDA) tests had been performed in coupons with and without the PVA-CNT fiber (reference).

Loading – unloading steps of the PDA tests ranged from four (4) up to eleven (11). Typical axial nominal stress – strain diagrams for the eleven incremental loadings for coupons without and with the PVA-CNT fiber can be seen in Figure 4(a) and (b), respectively. As the tests were load controlled after the unloading the specimen returned to its zero load (stress) condition. The incremental tensile loading steps of additional 50 MPa each, introduced damage to the material that can be noticed as residual strain measurements after every unloading step. Both networks of curves in the two Figures seem to be very similar. A more detailed approach to seek the differences in structural integrity of the different coupons can be assessed via introduced damage that can be expressed in these materials through stiffness degradation and residual strain measurements.

Damage develops to the composite with the incremental, quasi-static loading – unloading steps. Depending on the magnitude of the peak load value, different kind of damage is developed to the composite, e.g. for the low loading values, mainly matrix cracking and debonding between matrix and fibers happens; for medium loading values delamination occurs, while for loadings close to the ultimate tensile load, the main damage mechanism is fibre breakage. Location of the development of damage is strictly linked with the main damage mechanism of the composite. Briefly, with increasing loading, location of the damage occurs firstly in the matrix, then to the interface between the plies of the composite and the final step is the failure of the fibres.

Despite that the damage mechanisms are well known, there is no absolute measure amongst researchers to quantify damage. Pantelakis et al. used ultrasonics to quantify the developed damage in APC2 composites after fatigue testing [34], [35] and correlate the findings with residual mechanical properties of the material. Loutas and Kostopoulos used acousto-ultrasonics and acoustic emission techniques to quantify damage development in carbon/carbon, woven reinforced composites [36], [37]. Philippidis et al. classified acoustic emission signals from composites as to their origin in order to characterize each individual damage mechanism [38]. Recently, Aggelis et al. characterized the transition of the damage mechanism from transverse matrix cracking to delamination in cross-ply laminates using advanced AE indices [39],[40]. Nevertheless, from the mechanical point of view, developed damage to the composite can be calculated by the reduction of the modulus of elasticity or by the normalized modulus of elasticity  $E/E_0$ .

Figure 5 shows the decrease of the normalized modulus of elasticity for a number of coupons with incremental tensile loading steps. The test results for the coupons without and with embedded PVA-CNT fibers can be seen in the Figure, as well as the main damage mechanisms of the investigated composite. Stiffness decrease is almost the same for the specimens with and without embedded PVA-CNT fiber. It is also absolutely dependant on the number of loadings up to fracture and therefore by the introduced damage to the coupon; for the cases of low (4) and many (11) loadings, the stiffness degradation follows the same pattern regardless the presence or the type



of PVA-CNT fiber. Additionally, fracture of the specimens always initiated and occurred within the gauge length of the coupon and not in the wiring connections of the PVA-CNT fiber and given the scatter in composites, it can be concluded that the addition of the fiber didn't decrease the material's mechanical properties.

Figure 6 shows the introduced, residual axial strain measured after every unloading step of the coupon. It is not surprising that residual strain increases with the number of loading steps. This is explained by the higher introduced damage to the coupon due to the number of loadings. The measured residual strain is almost the same for the low number of loading steps (4) for all kind of coupons, Figure 6. This is also the case for the high number of loading steps in the coupons. Hence, the mechanism for accumulating damage is the same regardless the presence or type of the embedded PVA-CNT fiber.

#### ***4.2 Results for the pre-stretched CNT fiber***

Typical results of the various incremental loading – unloading steps of a coupon with embedded pre-stretched PVA-CNT fiber can be graphically seen in Figure 7(a). An example of six loading – unloading steps is shown to seek simultaneously the hybrid material's mechanical / electrical resistance response. The specific loading levels were 13%, 25%, 36%, 60%, 83% and 100% of the fracture stress, respectively. The PVA-CNT fiber's electrical resistance ( $\Delta R/R_0$ ) follows the mechanical response (stress-strain) of the coupon; it increases when loaded and decreases when unloaded.

As is shown graphically in Figure 3 for the case of untreated PVA-CNT fiber, the specific loading – unloading case resulted in a residual resistance of almost 1% of the PVA-CNT fiber. Larger residual resistance measurements of the order of 2% to 4% were noticed after higher level of incremental loading – unloading step. This is not the case for the pre-stretched PVA-CNT fibers, where after the six loading – unloading steps the residual resistance of the fiber is very small. Figure 7(a) shows that from the initial resistance of  $R_0 = 112.3 \text{ k}\Omega$ , the measured resistance before the 6<sup>th</sup> and final loading was  $R_6 = 112.9 \text{ k}\Omega$ , that corresponds to residual resistance of almost  $0.6 \text{ k}\Omega$  in  $112.3 \text{ k}\Omega \approx 0.5\%$ . In addition, the loading – unloading branch of the resistance change of the PVA-CNT fiber in the same Figure follows the same pattern; the two branches are hardly recognizable and are indicated via arrows. This didn't happen for the case of the GFRP material with embedded untreated PVA-CNT fiber; the loading and unloading resistance branches could be clearly distinguished, e.g. in Figure 3.

In [29] it was shown that the correlation between electrical resistance of the untreated PVA-CNT fiber and stress (or strain) of the material was loading history's dependant. According to the

damage occurred to the matrix of the composite due to the incremental loadings loops, this correlation altered; the higher the damage occurred to the material, the higher this variance of the correlation altered. For comparison purposes to the material with embedded untreated PVA-CNT fiber, the correlation between mechanical stress and electrical resistance change had been plotted in Figure 7(b) for the six incremental loading steps of the current test. The four distinguishable curves of the Figure seem to follow the same growth rule and no significant change is noticed for the present case. This is due to the nature of the current pre-stretched PVA-CNT fiber.

#### ***4.3 Comparison between the two different CNT fibers***

Typical mechanical strain – electrical resistance change diagrams for the two different types of PVA-CNT fibers can be seen in Figure 8. Untreated fiber coupon's loading-unloading steps can be seen in Figure 8(a) for 9 different steps till fracture. Each loading maxima is marked in the Figure, where a hysteresis loop is formed for all cases after unloading. Loading branch of each step follows always an exponential curve while unloading branch is always linear. This behavior was extensively discussed in [29] and was attributed to possible plastic deformation of the PVA material of the fiber. Besides the expected residual strain measurements after every unloading step, noticeable is also the residual resistance measurements of the untreated PVA-CNT fiber. Essential residual resistance measurement is recorded, with a maximum value of 4% at the last loading step. Critical value of residual resistance is the value of almost 0.5% presented after the fourth unloading. It actually represents the threshold value for damage detection of the composite.

On the contrary, the specimen with the embedded pre-stretched PVA-CNT fiber does not present a similar behavior. Typical diagram of strain – resistance correlation for different 4 loading steps can be seen in Figure 8(b). As presented earlier, the loading and unloading branch of each step is almost identical; there a hysteresis loop does not exist or exists at a very small scale. Noticeable is also the absence of large residual resistance measurements; for the present example it doesn't exceeded in total the 0.5% value.

An essential, direct comparison between the untreated and pre-stretched PVA-CNT fibers is assessed via three different cases; loading – unloading steps at (a) low, (b) medium and (c) high stress levels, where the damage mechanisms are matrix cracking, delamination and fibre breakage, respectively. The comparison between the different loading – unloading steps had been made on different specimens that had absolutely the same loading history. The electro-mechanical test results for the comparison purposes can be seen in Figure 9.

The first comparison set had been made in the low stress region; this was selected to be the 33% of the fracture stress of the coupon. Usually at this loading stress the damage mechanism of the

composite is debonding between fibres / matrix as well as initiation of matrix cracking. The electrical readings of the two fibers quite differ; for the untreated fiber a hysteresis loop is formed, while this is not observed for the pre-stretched fiber. Additionally, for the untreated fiber a residual resistance is observed, while this is not noticed for the pre-stretched fiber, Figure 9(a). At last, the untreated fiber presents higher value of resistance change  $\Delta R/R_0$  at the pre-defined stress; this value is almost double that the calculated value for the pre-stretched fiber at the same stress.

The second stress level was selected to be at the magnitude of 66% of the fracture stress of the coupon. At this stage of mechanical testing, an essential damage due to matrix cracking, debonding of the fibres has already been induced to the composite material, while delamination is occurring. Test results of the comparison are almost identical with the low stress level, Figure 9(b). Hysteresis loop and residual resistance after the unloading step is noticed for the untreated PVA-CNT fiber, while none of them is noticed for the pre-stretched fiber. Almost double values of  $\Delta R/R_0$  were again calculated for the untreated PVA-CNT fiber.

Those observations can be understood by considering that fiber stretching improves the mechanical properties of the fibers. In specific, it has been shown that fiber stretching increases the tensile strength and Young's modulus of previously investigated PVA-CNT fibers [32]. Such improvements could result in a better damage resistance, especially in very low tensile strains. This can explain thereby the absence of hysteresis behavior and very low values of residual resistance of the prestretched fibers. The lower values of  $\Delta R/R_0$  observed for prestretched fibers reflect a lower sensitivity to strain. This is in good agreement with the piezo-resistive behavior of single fibers at low strain. As shown in Figure 2, the prestretched fiber exhibits lower sensitivity to strain at their low strain regime.

Identical comparison results can be seen in Figure 9(c) for the high stress level (almost 87% of fracture stress). This loading step is very close to the final fracture of the material. As regards to the composite material, the damage mechanisms are mainly delamination growth and possibly fracture of the structural fibers.

#### ***4.4 Assessment of the measurements of the CNT fibers with material damage***

The PVA-CNT fibers were embedded into the composites for sensing and monitoring purposes. Hence, the electrical readings of the PVA-CNT fibers should be used and correlated directly to the composite's introduced damage; damage is interpreted in the current study by means of residual axial strain and decrease of the material's stiffness measurements.

Modulus of elasticity of the composite  $E_{\text{comp}}$  can be roughly calculated in the axial direction:

$$E_{comp} = E_f \cdot V_f + E_m \cdot V_m, \quad (1)$$

where  $E$  stands for modulus of elasticity,  $V$  for volume fraction and the subscripts  $f$  and  $m$  for fibers and matrix, respectively. Given that  $E_f = 60$  GPa,  $E_m = 2.4$  GPa and typical fiber volume fraction for the vacuum infusion method is  $V_f = 0.38$ , eqn (1) gives that the typical stiffness of the composite is  $E_{comp} = 24.29$  GPa, which is very close to the experimentally measured values. Taking into account that at the first damage stages of the composite, debonding and matrix failure occurs, a rough calculation of these stages can be attempted. Eqn (1) for the complete matrix failure  $V_m \approx 0$ , gives that the stiffness of the composite comes from the elasticity of the glass fibers and yields to values of the order of magnitude of 0.93 to 0.94. Hence, this is the theoretical transition point to the delamination stage, if only matrix failure occurred in the first service stages of the composite (Figure 5). As fibre breakage is the dominant failure mechanism before the macroscopic tearing of the composite, this stage can also be noticed in Figure 5 and typical the normalized modulus of elasticity takes values of less than 0.85. The most lasting damage stage in the composites is the delamination stage, and as a consequence it lies in values of  $E/E_0$  in between the before-mentioned stages, e.g. 0.94 to 0.85 for the investigated composite.

All the available experimental data for all types of PVA-CNT fibers can be seen in Figure 10 by means of the residual resistance measurements as a function of the percentage of fracture stress of the composite. Coupons with untreated fibers are marked as rectangular while the pre-stretched fibers as pyramid. For all cases, the residual resistance measurements of the PVA-CNT fiber are dependant by the number of loading-unloading steps. Similar behavior was also noticed in Figure 6 for all specimens when plotted residual axial strain and percentage of fracture stress. It is eminent that for a specimen that suffered high number of loading – unloading steps till fracture, greater accumulating damage will be introduced to the material.

The two fibers show a completely different trend in Figure 10; untreated fiber shows an exponential increase behavior while the pre-stretched fiber a fairly linear trend. Marked in the Figure are also the mean trend lines as well as the upper and lower limits for the two different fibers. The untreated fiber gives almost identical values for low-level loadings up to 50% with the pre-stretched fiber. Beyond this critical value, untreated fiber exhibits an essential increase that can be used for damage monitoring. On the contrary, the pre-stretched fiber exhibits for all values a linear behavior ( $R^2 = 0.97$ ) of the form

$$\left( \frac{\Delta R}{R_0} \right) = A \cdot (PERFRA), \quad (2)$$

where  $PERFRA$  is the percentage of fracture stress and  $A = 0,00643$  is a material/fiber constant. This means that the pre-stretched fiber prognoses a fairly linear increase in residual resistance (damage) with the incremental loading step, despite the damage mechanism of the composite.

To assess the introduced damage of the composite by means of the monitoring parameter  $\Delta R/R_0$ , Figure 11 can be plotted. It can be used to assess for known values of residual resistance the damage level of the composite via residual axial strain measurements. An exponential decrease fitting was used for the untreated fibers, while a linear form ( $R^2 = 0.96$ ):

$$(RESAS) = B \cdot \left( \frac{\Delta R}{R_0} \right), \quad (3)$$

can be used for the investigated coupons.  $RESAS$  stands for residual axial strain, while parameter  $B = 0.0882$  is the average increase rate of damage accumulation with electrical measurements. Common values for the two different fibers can be seen in Figure 11 only for low damage values, where debonding and matrix cracking degradation mechanisms are dominant. For the other damage mechanisms, the readings of the two PVA-CNT fibers quite differ.

The most popular damage indication of the composite by means of mechanical testing is the stiffness decrease. For this cause, the residual resistance measurements of the fibers were plotted in Figure 12 against their respective values of normalized modulus of elasticity  $E_i/E_0$ . Notice that the damage stages of matrix cracking and delamination are also marked in the Figure. For the case of the normal fiber, an exponential curve fit ( $R^2 = 0.96$ ) can be used, having the form:

$$\frac{E_i}{E_0} = C + D \cdot e^{-\left(\frac{\Delta R}{R_0}\right)^t}, \quad (4)$$

where  $C = 0.8293$ ,  $D = 0.16274$  and  $t = 0.76217$  are material / PVA-CNT fiber dependant constants. For the case of calibration of the investigated pre-stretched PVA-CNT fiber, the mean introduced damage for the investigated system of material and fiber can be fitted by the following linear regression ( $R^2 = 0.99$ ):

$$\frac{E_i}{E_0} = (REF) - (DAMRA) \cdot \left( \frac{\Delta R}{R_0} \right), \quad (5)$$

where the parameter  $REF$  equals to unity and  $DAMRA = 0.2463$  is the average damage rate of the specific composite. This linear correlation can be used in all stages of damage accumulation in composites, as graphically noticed in the respective Figure.

At the present stage and for the investigated PVA-CNT fibers, the pre-stretched fiber seems to be more promising to be used for sensing purposes in non-conductive composite materials. This is due to its almost linear correlation with the applied strain of the composite, as well as its loading-unloading behavior that presents no hysteresis loop. Nevertheless, the pre-stretched PVA-CNT fiber

presented no significant residual resistance values after the different unloading steps that might be very useful to monitor damage in the composite during different mechanical loadings.

#### *4.5 Discussion*

In the present work, it was shown that the embedded PVA-CNT fiber has the potential to be used for damage detection in GFRP composites. The fiber can be calibrated in order to be used as a strain sensor and to monitor the developed damage in composites with mechanical loadings. Still, there are many questions to be answered, e.g. regarding the sensitivity of the fiber to transverse cracks or when subjected to temperature and moisture effects. These topics are a matter of running research as well as the need to optimize the fiber's sensitivity to stress and strain variations. The optimization treatments includes the addition of salts (borate) to create hydrogen bonds between the PVA chains and pre-stretching treatments at different temperatures to increase the alignment of both the polymer chains and nanotubes.

## 5. Conclusions

- It is the first time that the embedded PVA-CNT fiber electrical resistance readings are directly correlated to induced damage of composites for structural health monitoring purposes. At the present study two different CNT fibers were used as sensors, having different advantages and disadvantages.
- The effect of pre-stretching enables this PVA-CNT fiber to be used as a sensor without leaving essential residual resistance of the fiber after every unloading. The resistance – strain correlation remains actually unaltered by the incremental loadings of the present study and the respective, induced damage to the material.
- The untreated fiber gives essential residual resistance after every unloading; however it still can be calibrated in order to monitor the induced damage to the composite. Disadvantage of this fiber is that the correlation between resistance and strain of the fiber alters with induced damage.
- The cyclic loading of the fibres led to the conclusions that pre-stretching of the fibres is resulting to a fairly linear behaviour of the fibre as a function of strain. The residual strain on the fibre is limiting the linear part of the curve during unloading.

## Acknowledgements

The experiments in the present work are part of the FP6 EU-STREP project NOESIS ‘Aerospace Nanotube Hybrid Composite Structures with Sensing and Actuating Capabilities’ (Project no AST4-CT-2005-516150), which was supported by the European Union.

## References

- [1] Boller, C., Chang, F.-K. and Fujino, Y., *Encyclopaedia of structural health monitoring*, John Wiley & Sons Ltd. (2009).
- [2] Balageas, D., Fritzen, C. and Guemes, A., Editors, *Structural Health Monitoring*, London; Newport Beach, CA: ISTE (2006).
- [3] Giurgiutiu, V., *Structural health monitoring with piezoelectric wafer active sensors*. Elsevier, Oxford (2008).
- [4] Park G, Cudney HH, Inman DJ. *Journal of Intelligent Material Systems and Structures*, 2000, 11, 448-455.
- [5] Pierce, S.G., Philp, W.R., Culshaw, B. Gachagan, A. McNab, A., Hayward, G. and Lecuyer, F. *Smart Mater. Struct.*, 1996; 5, 776-787.
- [6] Pardo De Vera, C. and Guemes, J.A. *Journal of Intelligent Material Systems and Structures*, 1998, 9,876-882.
- [7] Pohl, J., Herold, S., Mook, G. and Michel, F. *Smart Mater. Struct.*, 2001, 10, 834-842.
- [8] Garg DP, Zikry MA, Anderson GL, Stepp D. *Structural Health Monitoring*, 2002, 1, 23-39.
- [9] Inman DJ, Ahmadian M, Claus RO. *Journal of Intelligent Material Systems and Structures*, 2001, 12, 775-783.
- [10] Hurlebaus S, Gaul L. *Journal of Intelligent Material Systems and Structures*, 2004, 15, 729-736.
- [11] Ghoshal A, Chattopadhyay A, Schulz MJ, Thornburgh R, Waldron K. *Journal of Intelligent Material Systems and Structures*, 2003,14,521-537.
- [12] Giurgiutiu V, Zagrai A, Bao J. *Journal of Intelligent Material Systems and Structures*, 2004, 15, 673-687.
- [13] Hofer B., *Composites*, 1987, 18, 309-316.
- [14] Waite SR, Tatam RP, Jackson A., *Composites*, 1988, 19, 435-442.
- [15] Takeda S, Okabe Y, Takeda N., *Composites Part A*, 2002, 33, 971-980.
- [16] Park JM, Lee SI, Kwon OY, Choi HS, Lee JH., *Composites Part A*, 2003, 34, 203-216.
- [17] Leng J, Asundi A., *Sensors and Actuators A*, 2003, 103, 330-340.
- [18] Lee DC, Lee JJ, Yun SJ., *Comp. Struct.*, 1995, 32, 39-50.
- [19] Seo DC, Lee JJ., *Comp. Struct.*, 1995,32,51-58.
- [20] Prasse T, Michel F, Mook G, Schulte K, Bauhofer W., *Compos. Sci. Technol.*, 2001,61,831-835.
- [21] Katerelos, D.T.G., Paipetis, A., Loutas, T., Sotiriadis, G., Kostopoulos, V., Ogin, S.L., *Plastics, Rubber and Composites*, 2009, 38, 229-234.
- [22] Leone C, Caprino G, Iorio I., *Compos. Sci. Technol.*, 2006, 66, 233-239.
- [23] Loutas, T.H., Kostopoulos, V., *Compos. Sci. Technol.*, 2009, 69, 265-272.
- [24] Loutas, T.H., Kostopoulos, V., Ramirez-Jimenez, C., Pharaoh, M., *Compos. Sci. Technol.*, 2006, 66, 1366-1375.
- [25] K. Schulte, Ch. Baron: *Compos. Sci. Technol.*, 1989, 36, 349-56.
- [26] Irving, P.E. and Thiagarajan, C., *Smart Mater. Struct.*, 1998, 7/4, 456-66.
- [27] Arby, J.C., Bochart, S., Chateauminois, A., Salvia, M. and Giraud, G., *Compos. Sci. Technol.*, 1999, 59, 925-35.
- [28] Muto, N., Arai, Y., Shin, S.G., Matsubara, H., Yanagida, H., Sugita, M. and Nakatsuji, T., *Compos. Sci. Technol.*, 2001, 61, 875-883.
- [29] Alexopoulos, N.D., Bartholome, C., Poulin, P. and Marioli-Riga, Z., *Compos. Sci. Technol.*, 2010, 70, 260–271.
- [30] Vigolo, B., Penicaud, A., Coulon, C., Sauder, C., Paillet, R., Journet, C., Bernier, P. and Poulin, P., *Science*, 2000, 290, 1331-1334.
- [31] Poulin, P., Vigolo, B. and Launois, P., *Carbon*, 2002, 40, 1741.



- [32] Miaudet, P., Badaire, S., Derré, A., Maugey, M., Pichot, V., Launois, P., Poulin, P. and Zakri, C., *Nanoletters* 2005, 5, 2212-2215.
- [33] Lachman, N., Bartholome, C., Miaudet, P., Maugey, M., Poulin, P. and Wagner, D., *J. Phys. Chem. C*, 2009, 113, 4751–4754.
- [34] Pantelakis, Sp.G., Kyriakakis, Em.Ch., Papanikos, P., *Fatigue and Fracture of Engineering Materials and Structures*, 2001, 24 (10), 651-662.
- [35] Pantelakis, S.G., Kyriakakis, E.C., *Theoretical and Applied Fracture Mechanics*, 1999, 32 (1), 37-46.
- [36] Loutas, T.H., Kostopoulos, V., *Compos. Sci. Technol.*, 2009, 69 (2), 265-272.
- [37] Loutas, T.H., Kostopoulos, V., *Compos. Sci. Technol.*, 2009, 69 (2), 273-283.
- [38] Philippidis, T.P., Assimakopoulou, T.T., *Compos. Sci. Technol.* 2008, 68 (15-16), 3272-3277.
- [39] Aggelis, D.G., Barkoula, N.M., Matikas, T.E., Paipetis, A.S., *J. Acoust. Soc. Am.*, 2010, 127 (6), 246-251.
- [40] Aggelis, D.G., Barkoula, N.M., Matikas, T.E., Paipetis, A.S., *Proc. SPIE*, Vol. 7649, 764911 (2010); doi:10.1117/12.847600.

ACCEPTED MANUSCRIPT

## List of Figures

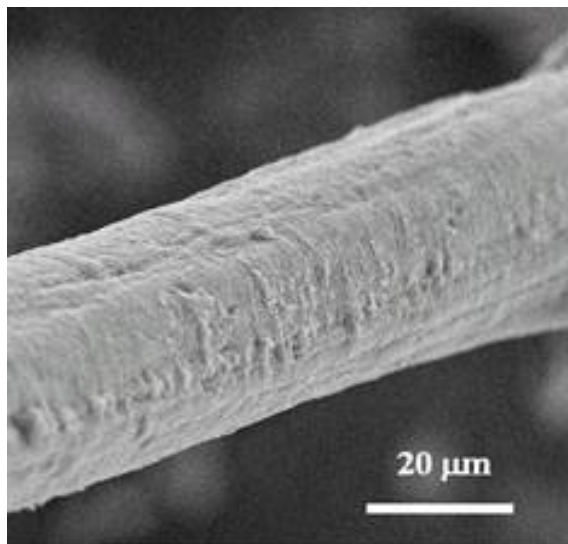


Figure 1: Scanning electron micrograph of a polyvinyl alcohol-carbon nanotube fiber.

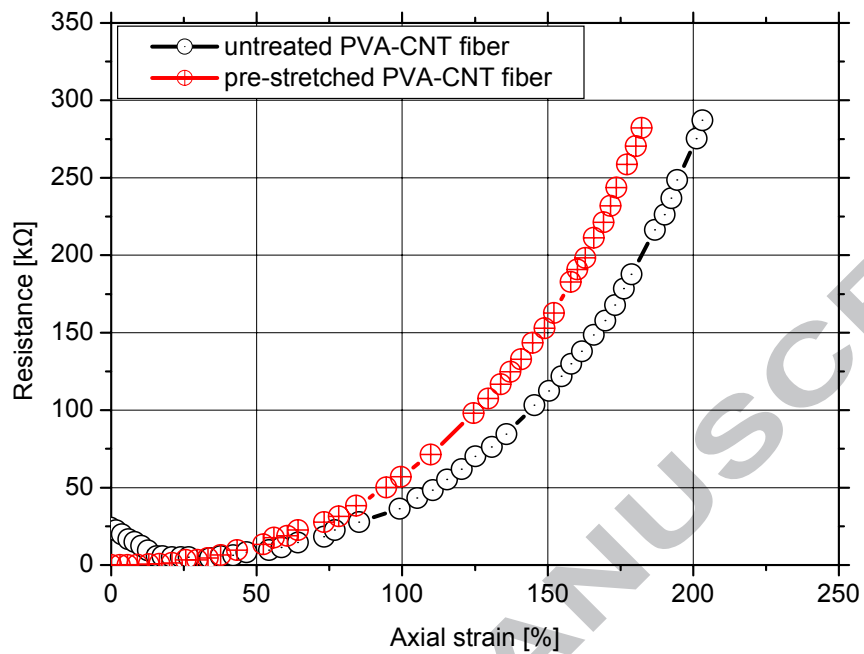


Figure 2: Typical resistance versus strain measurements for a monotonic loading till fracture of the different PVA-CNT fibers.

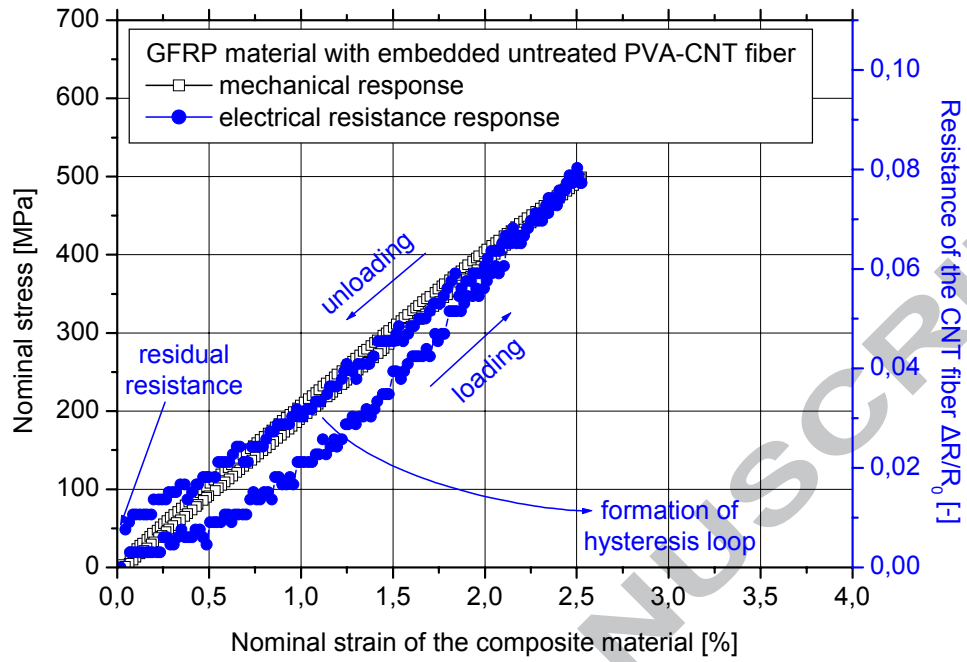
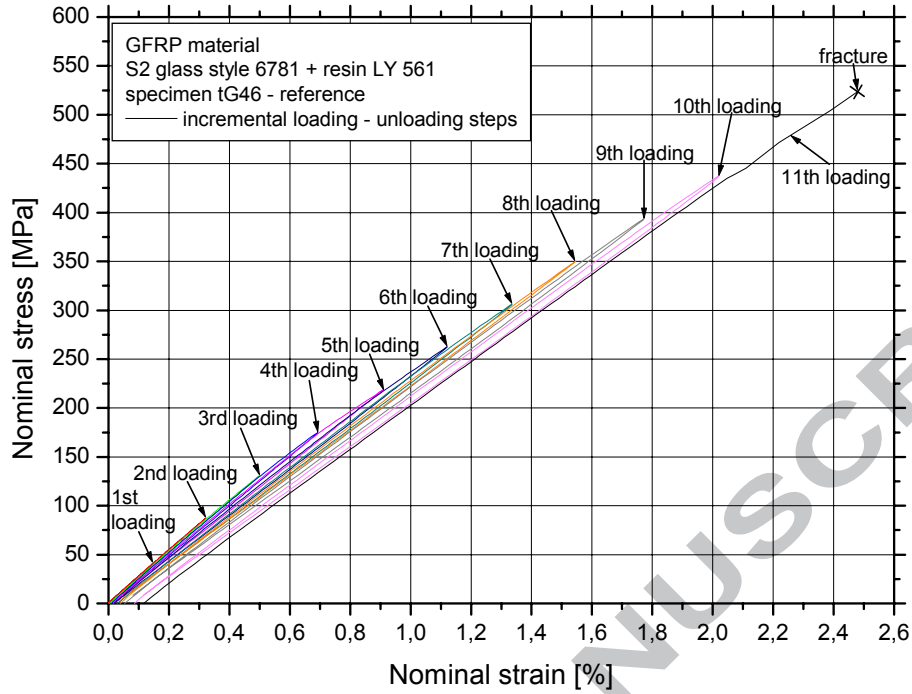
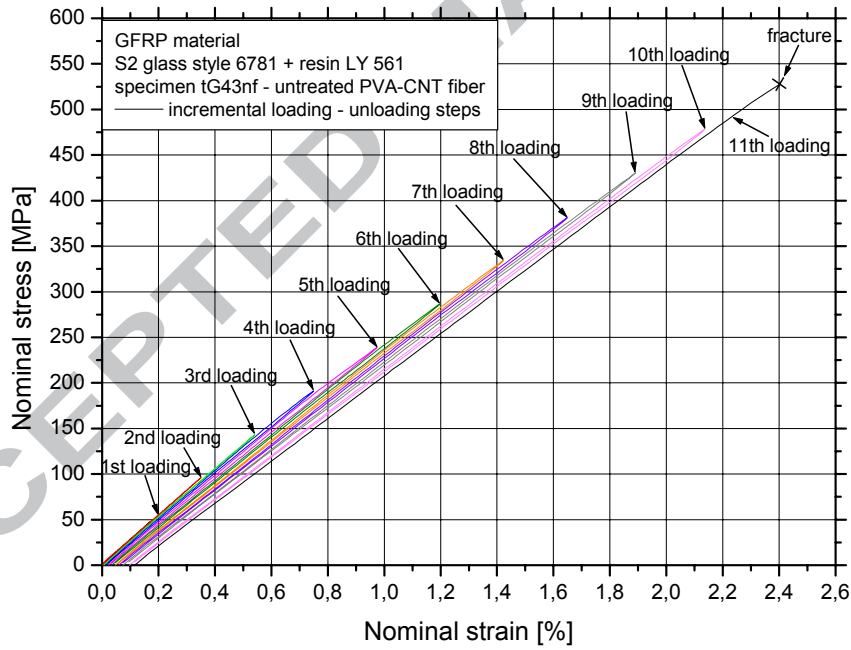


Figure 3: Typical loading – unloading resistance change curve of the embedded untreated PVA-CNT fiber in the GFRP specimen.



(a)



(b)

Figure 4: Nominal stress – strain curves for different loading – unloading steps of (a) reference GFRP coupon and (b) GFRP coupon with embedded untreated PVA-CNT fiber.

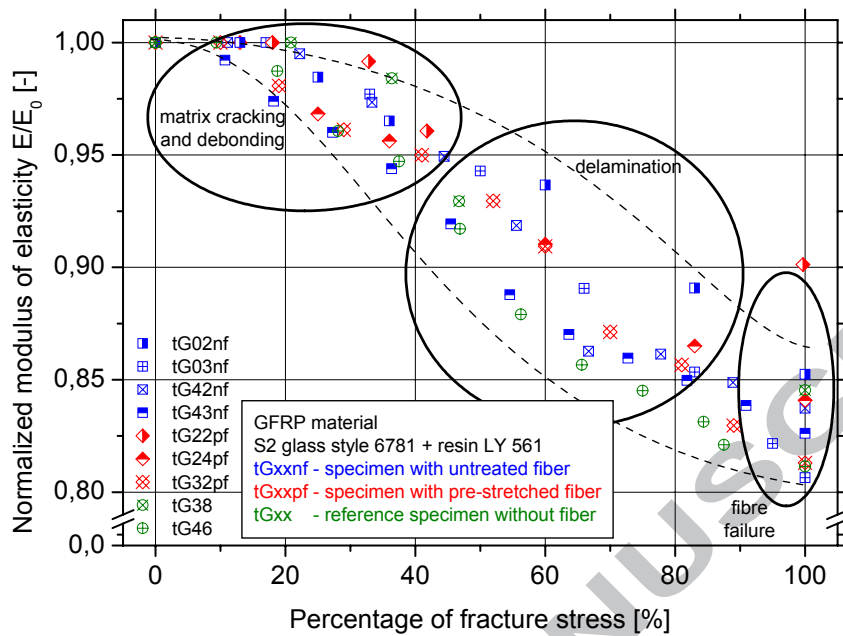


Figure 5: Modulus of elasticity degradation due to progressive damage accumulation tests of all investigated GFRP coupons.

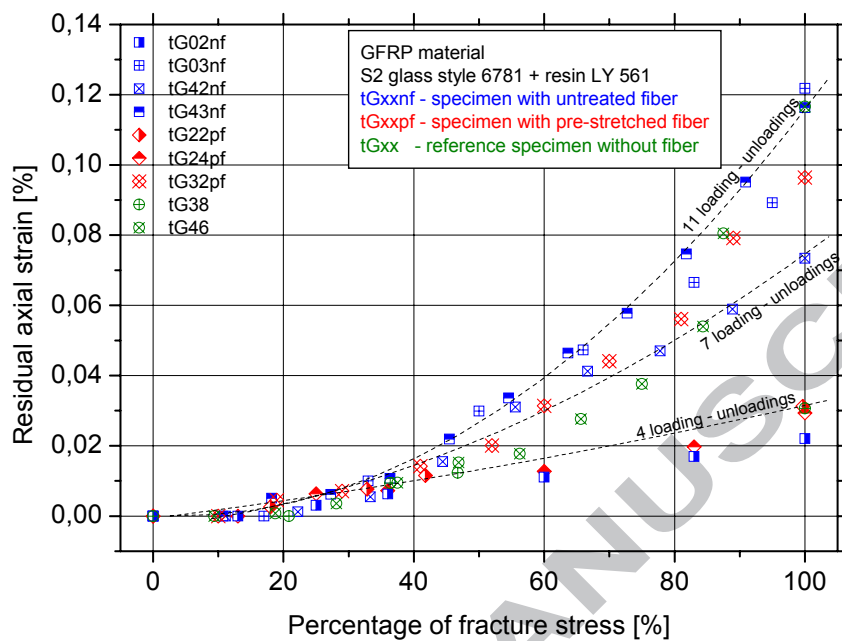
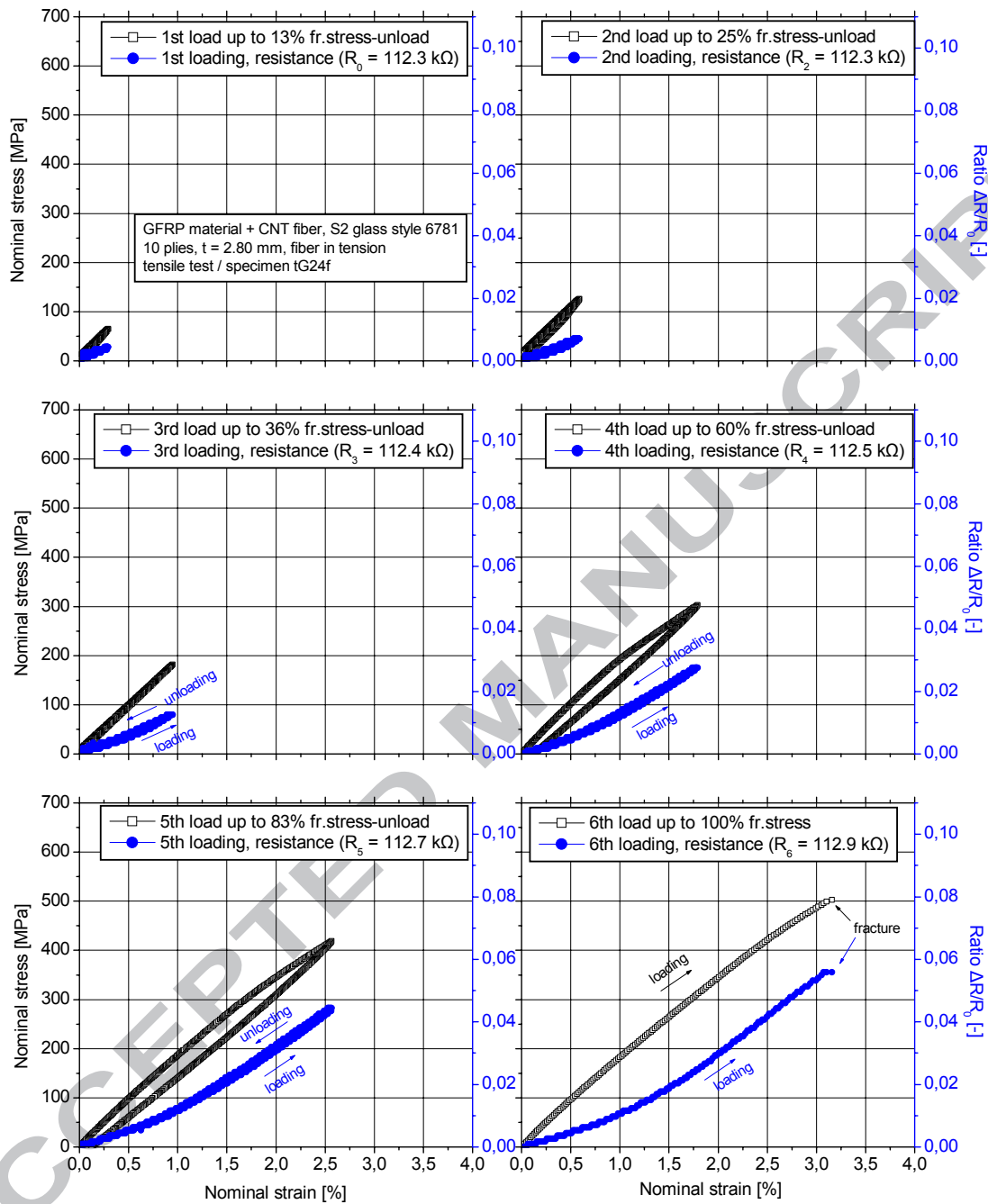


Figure 6: Measured residual axial strain for the progressive damage accumulation tests.



(a)



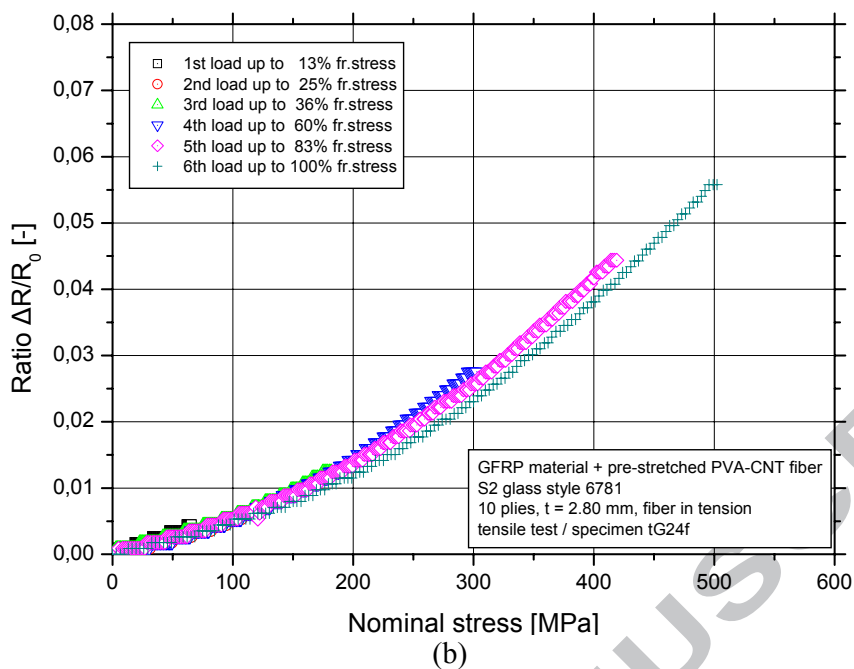
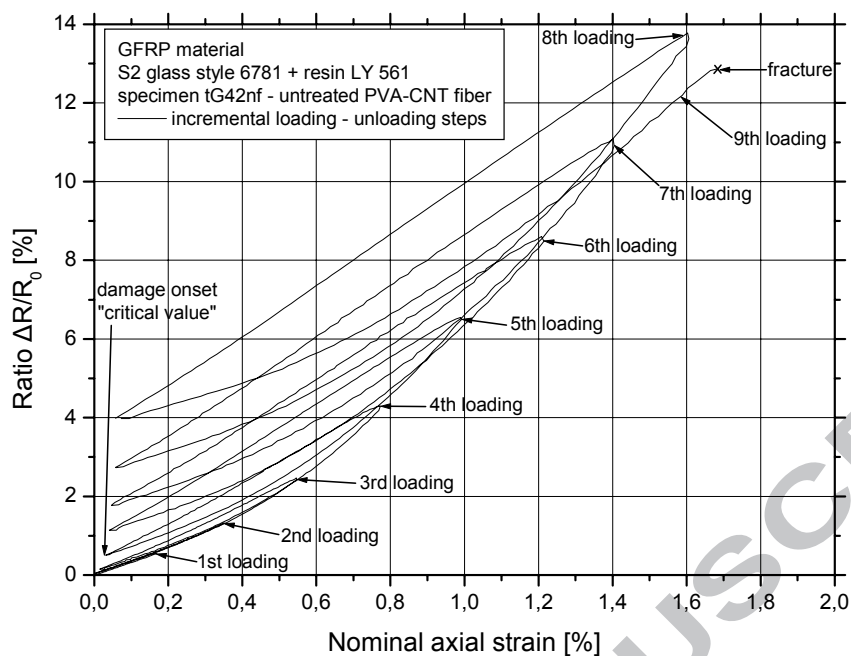
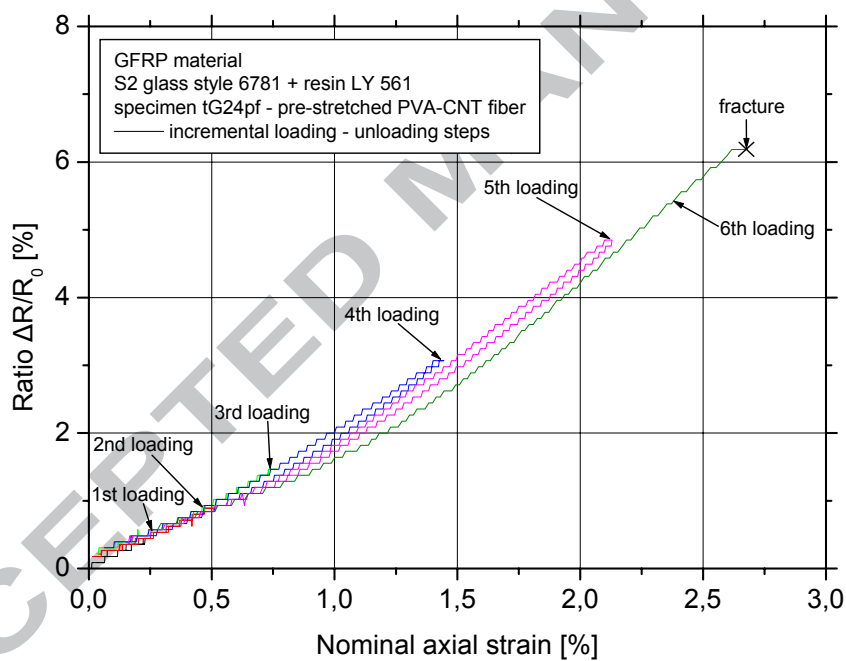


Figure 7: (a) Typical tensile mechanical and resistance results of a GFRP specimen with embedded pre-stretched PVA-CNT fiber for different incremental loading – unloading steps and (b) direct correlation between mechanical stress and electrical resistance  $\Delta R/R_0$  measurements.



(a)



(b)

Figure 8: Mechanical strain and electrical resistance  $\Delta R/R_0$  measurements for the GFRP material with embedded (a) untreated and (b) pre-stretched PVA-CNT fiber.

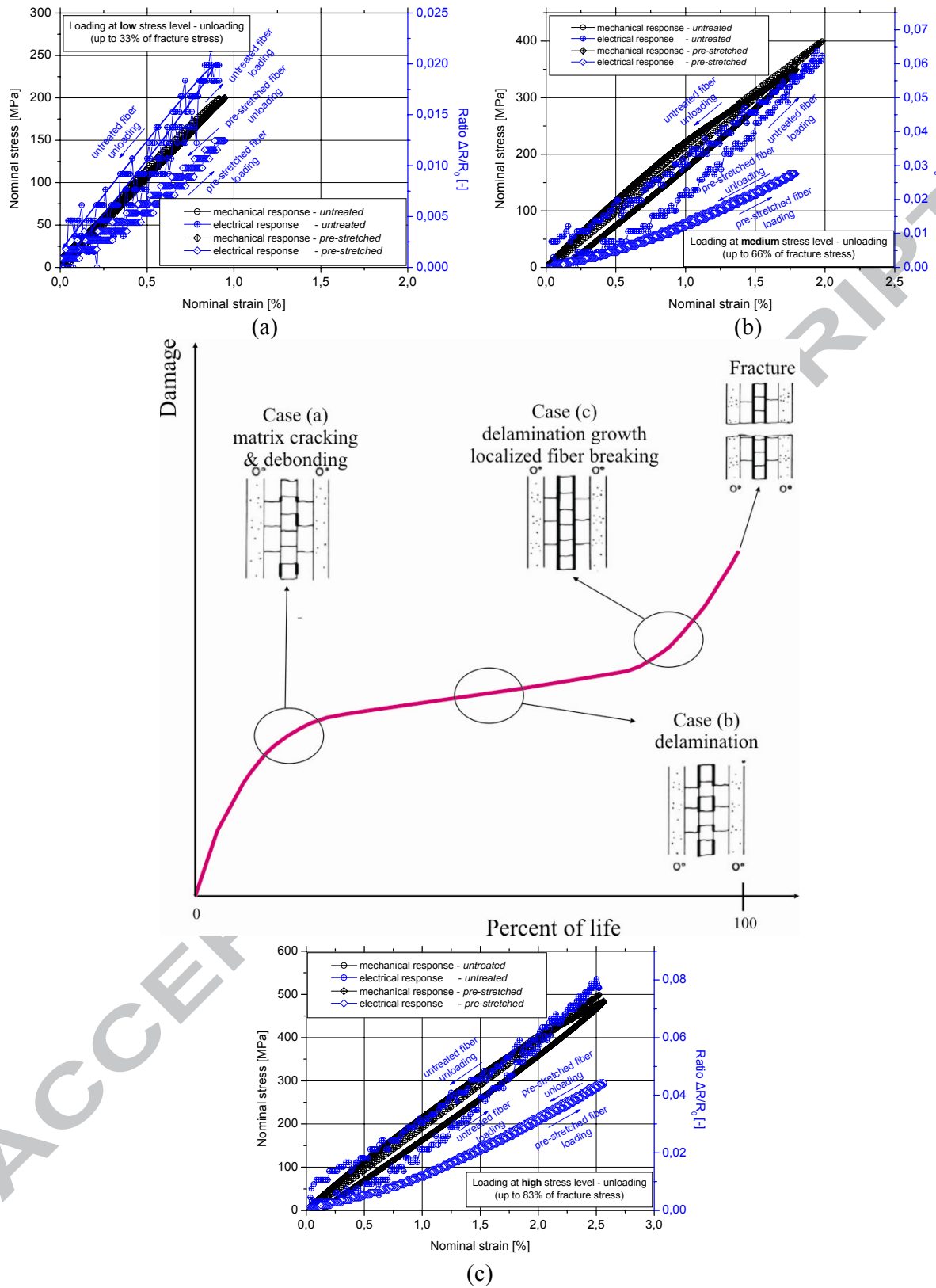


Figure 9: Mechanical and resistance change measurements of GFRP materials with embedded untreated and pre-stretched CNT fiber at (a) low, (b) medium and (c) high stress level loadings. All coupons had the same loading history.

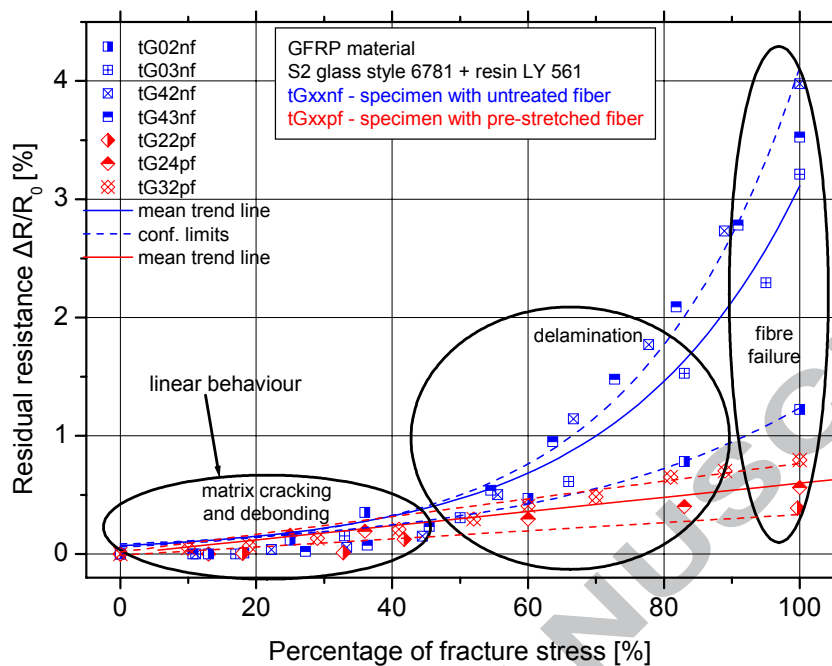


Figure 10: Correlation of the levels of incremental loading steps with residual resistance measurements of the PVA-CNT fiber.

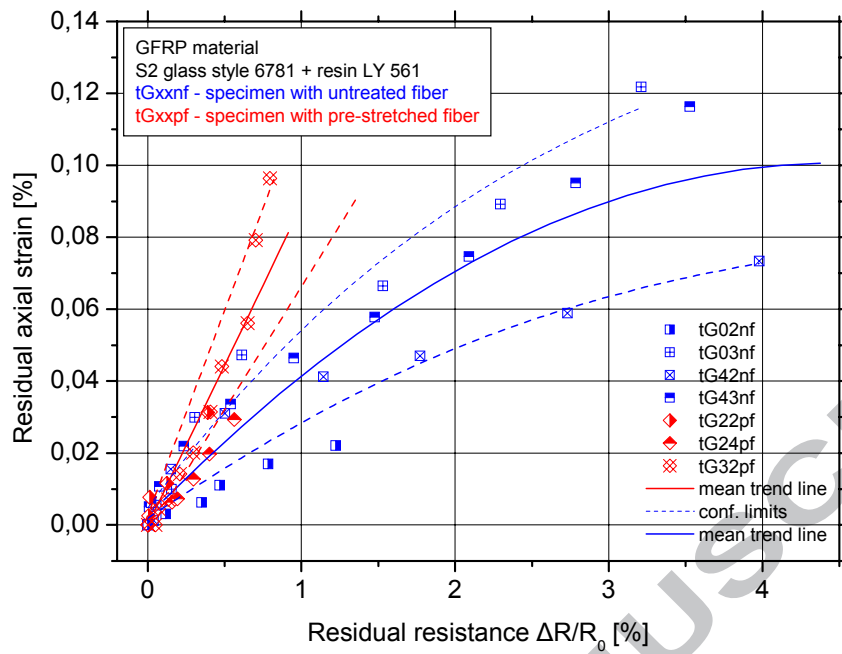


Figure 11: Measurements of damage of the composite by means of residual axial strain with the electrical readings of the two different embedded sensors.

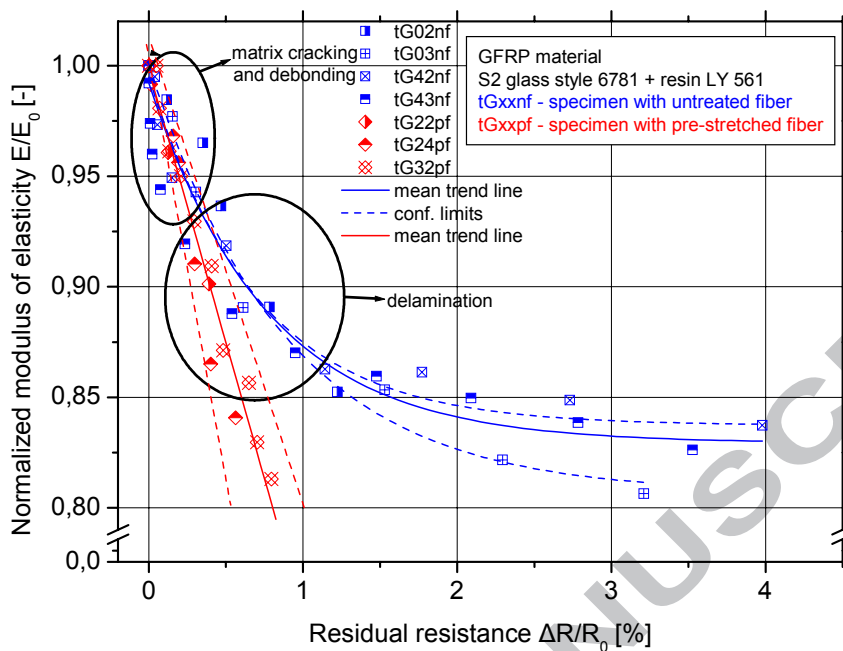


Figure 12: Correlation of the residual resistance readings with induced damage to the composite via normalized modulus of elasticity.